

# Structure and function of cells in a neural integrator

Ashwin Vishwanathan,<sup>1</sup> Kayvon Daie,<sup>3</sup> Alejandro D. Ramirez,<sup>3</sup>  
Jeff W Lichtman,<sup>4</sup> Emre Aksay,<sup>3</sup> and H. Sebastian Seung<sup>1,2</sup>

<sup>1</sup>Neuroscience Institute and <sup>2</sup>Computer Science Department  
Princeton University, Princeton, NJ 08544

<sup>3</sup>Institute for Computational Biomedicine and  
Department of Physiology and Biophysics,  
Weill Cornell Medical College, New York, NY 10021

<sup>4</sup>Department of Molecular and Cellular Biology and Center for Brain Science,  
Harvard University, Cambridge, MA 02138

July 1, 2016

## Abstract

Neural integrators are involved in a variety of sensorimotor and cognitive behaviors. The oculomotor system contains a simple example, a hindbrain neural circuit that takes velocity signals as inputs, and temporally integrates them to control eye position. We combined observations of behavior, physiology, and anatomy to study integrator neurons. To understand the mechanisms of integration, here we performed ultra-structural analysis of functionally-identified neurons located in the neural integrators. Two-photon calcium imaging of the larval zebrafish hindbrain was performed while simultaneously monitoring spontaneous eye movements. Integrator neurons were identified as those cells with activities highly correlated with eye position, and the same neurons were then reconstructed from serial electron microscopic images. Three major morphological classes of cells were observed: ipsilaterally projecting cells located medially and rostrally, contralaterally projecting cells located more laterally and caudally, and a population at the extreme lateral edge of the hindbrain for which we were not able to identify axons. Based on previous reports of correlation between somatic location and neurotransmitter identity, we infer that cells with only ipsilaterally projecting axons are largely glutamatergic and excitatory, whereas cells with only contralaterally projecting axons are largely GABAergic and inhibitory. Dendritic and synaptic organization of the ipsilaterally projecting cells suggest a broad sampling from inputs on the ipsilateral side. Finally, we observed the first conclusive evidence of synapses between integrator neurons, from an ipsilaterally projecting cell onto other cells. These results support the idea of integration through positive feedback by recurrent excitation.

## 1 Introduction

The larval zebrafish has become an important model organism for investigating the relation between neural circuits and behavior [Friedrich et al., 2010]. Whole animal neural activity has been observed via calcium imaging and correlated with a variety of behaviors [Ahrens et al., 2012]. However, understanding the neuronal and network underpinnings of these behaviors has been difficult to address due to lack of approaches that connect cellular and circuit structure with global function. Recent developments in the mouse retina [Briggman et al., 2011] and primary visual cortex [Bock et al., 2011, Lee et al., 2016], using 3d electron microscopic reconstructions along with two-photon calcium imaging have begun to address such questions.

Here we implement such an approach in the larval zebrafish to investigate the ultra-structure of cells that generate persistent firing in a hindbrain neural circuit known as the "velocity-to-position neural integrator," or "neural integrator" for short [Major and Tank, 2004, Joshua and Lisberger, 2015]. The neural integrator gets its name because the transformation of eye velocity into eye position is the computational operation of integration with respect to time. Integrator cells are operationally defined as premotor neurons that carry a horizontal eye position signal in their spiking.

(There is also an integrator for vertical eye movements, but it will not be discussed here.) Integrator cells are thought to send their eye position signals through direct synapses onto extraocular motor neurons in the ipsilateral abducens nucleus. They are also thought to receive signals from multiple convergent pathways that encode eye velocity for every type of eye movement. Therefore, the neural integrator is the “final common pathway” for all types of eye movements in fish [Pastor et al., 1994, Aksay et al., 2000, 2001], rodents [van Alphen et al., 2001], non-human primates [Robinson, 1989, Newcombe, 2008], and humans [Leigh and Zee, 2015]. We combined two-photon calcium imaging of neurons in a behaving fish to identify persistent firing cells in the neural integrator, with subsequent reconstructions of the same neurons using serial electron microscopy. The behavior is spontaneous eye movements, and the neurons are in a hindbrain neural circuit known as the “velocity-to-position neural integrator,” or “neural integrator” for short [Major and Tank, 2004, Joshua and Lisberger, 2015]. Previous attempts to understand how the integrator transforms a ‘pulse’ like input to a ‘step’ like output have relied on combining single-cell electrophysiology with light-microscopic dye fills. Intracellular recording in goldfish hindbrain neurons that exhibited spiking correlated to eye position, followed by anatomical dye fill, showed the axons of these cells to send collaterals to areas where other integrator cells were observed [Aksay et al., 2000]. Similar anatomical observations have been observed in cats [McCrea and Baker, 1985] and nonhuman primates [Steiger and Büttner-Ennever, 1979]. These observations have driven theoretical models that have proposed that integration can be setup by recurrent excitation between neurons [Kamath and Keller, 1976, Seung, 1996, Seung et al., 2000, Fisher et al., 2013]. More recent high throughput methods have relied on two-photon calcium imaging to identify many integrator neurons followed by sparse, targeted single cell electroporation of fluorescent indicators for anatomical reconstruction [Lee et al., 2015]. While these studies have delineated the arborization and projection patterns of integrator neurons, they were limited to one or a few neurons in any individual brain and do not reveal locations, distributions of synapses. And although, the axonal projections could potentially contact dendrites of other integrator neurons, conclusive evidence for contact and synapses has been lacking.

We firmly demonstrate structure and function links in the neural integrator by combined two-photon calcium imaging of integrator neurons during spontaneous eye movements, with subsequent reconstructions of the same neurons using serial electron microscopy. We found evidence for multiple classes of cells within the integrator population based on differences in arborization, projections and synaptic densities. These classes of cells include cells with ipsilaterally projecting axons, identified by the existence of presynaptic boutons containing vesicles, cells with only contralaterally projecting axons. In addition, we found cells at the lateral most edge of the volume, for which we could not identify an axon and a small subset of previously unreported integrator neurons with axonal arbors that were both ipsilateral and contralateral. We identified chemical synapses in our images by the existence of presynaptic vesicles and postsynaptic densities. All chemical synapses involving integrator neurons contained small vesicles, suggesting the presence of conventional rather than peptidergic neurotransmitters. We inferred the neurotransmitter identity of the cells, based on the organization of cell somata in the hindbrain into ‘stripes’ that correspond to the neurotransmitter identity [Higashijima et al., 2004, Kinkhabwala et al., 2011, Koyama et al., 2011]. On this basis, we inferred that integrator neurons with only ipsilaterally projecting axons are glutamatergic, and those with only contralaterally projecting axons are GABAergic. Finally we report evidence for synaptic connectivity between integrator neurons with ipsilaterally-projecting axons and between ipsilateral and contralateral projecting axons.

Our work is the first application of this approach to a population of neurons defined by their encoding of behavioral variables, rather than stimulus variables.

## 2 Results

### 2.1 Combined two-photon and electron microscopy of integrator neurons

To identify putative integrator neurons we performed two-photon calcium imaging of the caudal hindbrain in a x dpf larval zebrafish following bolus loading of the calcium sensor Oregon Green BAPTA 1-AM. [describe imaging plane specs here, focused on left side where loading was best]. Following functional imaging, we imaged the entire hindbrain of the animal with optical sections that were  $1\text{ }\mu\text{m}$  apart, producing a light microscopic volume (LM volume). Calcium signals were correlated with eye position to identify integrator somata from the imaged planes (Fig. 1A) [Miri et al., 2011b]. Cells were identified as integrator neurons if saccade-triggered average fluorescence was correlated strongly with saccade-triggered eye position following an ipsiversive saccade (Fig. 1A - b, arrow) (Pearson coefficient  $> 0.6$ ), the cell was identified as an integrator neuron (Fig. 1A - b). This resulted in the identification of 22 integrator cells from 3 distinct imaging planes.

As seen by the average of the fluorescence response (Fig. 1A- c), these cells have distinct, graded persistent activity during eye fixation. This persistent activity was quantified with a persistent firing metric, calculated as the area under an exponential fit to the firing rate profile determined from a deconvolution of the fluorescence data (methods). Overall, we observed that cells that were nearer to each other have similar persistence levels with cells at caudal locations having slightly higher persistence levels as compared to cells at rostral locations ( Sup. Fig. 1A ). As observed previously, the degree of persistent firing was distributed over a wide range (Figure 1A, D and Sup. Fig. 1B ). This result is consistent with the spatial organization of integrator cells in the larval zebrafish revealed by optical imaging [Miri et al., 2011a], and from paired unit recordings in goldfish and monkey[Aksay et al., 2003, Dale and Cullen, 2015].

After functional identification of neural integrator cells, the tissue was fixed and sectioned for serial electron microscopy, imaged at  $5\times 5\times 45\text{nm}$  resolution. These images were stitched and aligned to create a 3D electron microscopy volume (EM) that was registered with the LM volume. (Fig. 1B and Methods). The resulting EM volume extended ventrally from the Mauthner cell axon plane by  $\sim 60\mu\text{m}$ , caudally from the border of rhombomere 5/6 by  $\sim 200\mu\text{m}$  and laterally from the midline by  $\sim 100\mu\text{m}$ . The LM and EM volumes were registered to each other by an affine transform, producing correspondence of labeled cells and blood vessels (Fig. 1C). The soma of all 22 integrator cells from the LM volume were located in the EM volume within the rhombomeres 6,7 and 8 (Fig 1D). This procedure revealed three loosely organized groups of cells (addressed later) in the imaged volume. Overlaying the persistence 'level' of integrator cells revealed these groups to have cells with a large range of persistence levels.

## 2.2 Inferring neurotransmitter identity of integrator neurons

We attempted to infer neurotransmitter identity of the identified integrator cells based on their somatic locations. Cell bodies in the hindbrain of the larval zebrafish follow a stereotypic alternating stripes pattern of cell bodies and neuropil. Cells in the same stripe largely share the same neurotransmitter identity, and morphology [Higashijima et al., 2004, Kinkhabwala et al., 2011, Koyama et al., 2011]. We projected the locations of all cell somata (Fig. 1D, '+' symbol) from the imaged area onto a single plane and noticed the emergence of alternating peaks of cell somata and neuropil, reminiscent of the stripe like pattern. We were able to locate 3 peaks, each corresponding to a likely stripe (Fig. 1D, bottom panel). Based on this, we inferred the putative neurotransmitter identity of the integrator cells. The medial most peak on the ipsilateral side overlaps with cells that were shown to express the *alx* transcription factor, and are mostly glutamatergic [Kimura et al., 2006]. Cells in this peak were previously shown to almost exclusively contain glutamatergic integrator cells [Lee et al., 2015]. The intermediate peak corresponds to cells shown to express the transcription factor *dbx1b* [Kinkhabwala et al., 2011]. Integrator cells with a majority expressing glutamate and some expressing GABA have been reported along this stripe, with the a preference for dorsal cells to be glutamatergic, and ventral cells expressing GABA [Lee et al., 2015]. The lateral most peak of cells corresponds with the expression of the *barhl* transcription factor, which is also thought to be glutamatergic [Colombo et al., 2006, Kinkhabwala et al., 2011].

## 2.3 Anatomical properties of integrator cells

After the identification of the integrator cells in the EM volume, we then reconstructed all 22 cells and annotated the synaptic locations for all cells. We first characterized some of the anatomical properties that were common to all integrator cells. The high-res EM volume contained a total of 2967 somata spread over rhombomeres 5 through 8 ( Fig. 1D). The volume also contained well-known landmarks like the Mauthner cell [Lee et al., 1993], the axon of the contralateral Mauthner cell, cells MiD2 and MiD3 of the reticulo-spinal network [Lee et al., 1993], and a number of commissural bundles (Fig. 1D).

### Somata

The soma locations of the 22 integrator cells ended up in three loosely observed groups. These cells were distributed over  $\sim 23\text{ }\mu\text{m}$  in the dorsoventral axis and the entire rostrocaudal extent of the imaged volume. The first group of cells was located very close to the midline and at the rostral edge of the imaged volume, very close to the border of rhombomeres 6,7. The second group of cells was located at the caudal end of the imaged volume, lateral to the first group of cells, located in rhombomere 8, roughly between myotomes 1,2. A third loose group of cells was located at the lateral end of the volume in rhombomere 8. (Fig. 1D, colored circles). The diameters of the integrator cells were normally distributed, with a mean of  $4.5 \pm 0.6\text{ }\mu\text{m}$  (mean  $\pm$  standard deviation). In general, the size of the somata was proportional to the persistence level of the cells, with larger cells exhibiting higher degree of persistence (Sup. Fig.

1B). On average  $3.3 \pm 1.5$  neurites emerged from the somata, and traveled ventrally. Some neurites exited the imaged volume, leading to incompletely reconstructed cells.

## Synapses

We annotated 406 presynaptic (green circles, Fig. 2) and 2229 postsynaptic sites (red circles, Fig. 2) on integrator neurons. Synapses were identified by the presence of a presynaptic vesicle pool and an opposing postsynaptic density. Synapses from or onto integrator neurons contained small vesicles, presumably containing a conventional neurotransmitter. Elsewhere in the volume we did identify synapses with dense core vesicles, presumably containing a peptide neurotransmitter (Sup. Fig. 2A).

- Integrator postsynaptic sites

The postsynaptic densities were observed as a darkening of the membrane, indicative of more electron dense regions. The number of presynaptic sites on a cell averaged  $58 \pm 44.39$ . This is an underestimate of the number of output synapses from an integrator neuron, because most axonal arbors were cut off by the borders of the volume. If statistics are restricted to the 3 cells that were more complete than others, there were  $156 \pm 47.46$  postsynaptic sites.

- Integrator presynaptic sites

The presynaptic site was generally at a varicosity in the axon with vesicles throughout. Opposing the postsynaptic density, a small, denser cluster of vesicles was typically observed, along with the presynaptic density. These features are consistent with the idea of a presynaptic active zone. The number of postsynaptic sites on a cell averaged  $101 \pm 74$ . This is a reasonable estimate of the number of input synapses to an integrator neuron, because most dendritic arbors were reconstructed in their entirety. If statistics are restricted to the 3 cells that were more complete than others, there were  $97 \pm 38$  presynaptic sites.

- Tight Junctions

Along the somatic membrane, a darkening of the membrane interrupted by small gaps was often observed (Sup. Fig. 2B). The darkening persisted over multiple serial sections, suggesting that it was not an artifact of tissue preparation or imaging. We speculate that these darkenings are tight junctions, or electrical synapses, which are known to exist in the developing larval zebrafish hindbrain [Jabeen and Thirumalai, 2013]. These darkenings were visible between somata of integrator-integrator and integrator-non-integrator cells.

## Dendrites

Dendrites were defined by the absence of presynaptic vesicles and the presence of postsynaptic densities. They were mostly oriented ventral to the location of the somata. Dendrites were smooth rather than spiny. The dendritic arbors of these cells fell into a distribution with a long tail, see distribution of arbor size (Sup. Fig. 1). Cells with small arbors were completely reconstructed and did not have any dendrites that exited the imaged volume.

## Axons

We defined axons as neurites with presynaptic vesicles. No axons were observed emerging directly from the cell body. Instead, dendrites bearing postsynaptic sites turned into axons with presynaptic sites. This region of transition, from dendrite to axon, we termed axon initiation site. Example axon initiation sites are indicated in Fig. 2, showing the dendrite (neurite with red postsynaptic sites) turning into axons at the axon initiation (open arrow). The main trunk of the axon extended rostrally and ventrally (Fig. 2 A,B,C). From the main trunk emerged mediolateral branches, which we will term collaterals. Those at the rostral extreme of the volume appeared to overlap with the expected location of the abducens motor nucleus (based on its known position within rhombomere r5,6). In total, we reconstructed 1.62 mm of axonal length in the imaged volume.

We observed dark sheaths around some axonal segments. In some locations, we saw evidence that the sheath wrapped around the axon multiple times (Fig. 2A, EM panel), so we inferred that the axons were loosely myelinated, as compared to the thick dark myelin that is seen elsewhere in the volume. The axon of the cell in Fig. 2A was intermittently loosely myelinated along its rostrocaudal section. Mediolateral collaterals emerged from the gaps in loose myelin, and remained unmyelinated. Loose myelin sheaths have been previously reported in goldfish [Rosenbluth and Palay, 1961].

### Small protuberances

A small fraction (3% or 89/2229) of the postsynaptic sites were located on finger-like projections from dendrites that were enveloped by invaginations of axonal boutons (Fig. 2B, EM panel 2). These projections resemble structures found across multiple species called spinules, and are thought to be present on large, active synapses [Petralia et al., 2015]

Another interesting feature observed on all integrator cells was the presence of a primary cilium in all the 22 integrator cells. This cilium, typically  $< 1 \mu\text{m}$ , is enriched with microtubules, and emerges from the cell body very close to the Golgi complex. In some cases, this primary cilium terminated inside processes that were presumed glial (Sup. Fig. 3A). Orientation of primary cilium in integrator cells did not show any orientation preference (Sup. Fig. 3B)

### Putative axons

For some of the integrator cells the putative axons were identified. All putative axons crossed the midline at locations ventral to the somata. They were identified not based on the presence of vesicles opposed to post-synaptic densities, instead they were identified by non-conventional anatomical features. The features were as follows, firstly the putative axons were devoid of any postsynaptic sites on the ipsilateral side. Secondly, before crossing the midline, the putative axon became engulfed by processes that appeared glial in nature (Fig. 2 C,D). Thirdly, these putative axons were smaller than the remaining neurites of the cell. These are features typical of axons. The lack of presynaptic sites on these putative axons is similar to the initial segment of axons that were identified by the presence of vesicles, where no presynaptic terminals in the proximal part of the axon were observed, and presynaptic sites emerged only distally. The glial engulfment is consistent with the idea of glial bridges that are instrumental in the guidance of axons during development [Barresi et al., 2005]. Finally, the diameter of these putative axons were smaller to the other neurites and were similar to the diameters of conventional axons (Sup. Fig. 1C). The mean axonal diameter was less than the mean dendrite diameter, conforming to the textbook notion that axons are thinner than dendrites (addressed later). All but one integrator cell with contralaterally projecting putative axons did not emerge from the somata of the cell. Instead, the initial zone of the putative axon contained postsynaptic sites (Fig. 2 C,D - postsynaptic sites before putative axon). Furthermore, since neurite diameters are close to the diffraction limit, light microscopic estimation of neurite diameters could be inaccurate.

## 2.4 Axonal projection patterns of integrator cells

We divided the reconstructed integrator cells into four groups based on their axonal arbors, as described below.

Ipsilateral projection only ("ipsi-only") - Six cells located at the rostral edge of the volume, were observed to have only ipsilaterally projecting axons (Fig. 3A). Two representatives are shown in Figs. 2A and B. The axons were clearly identified by the presence of *en passant* boutons with presynaptic vesicles. The cell bodies were located at the rostral extent of the volume, and close to the midline (Fig. 3A, Ipsi. only). The average length of all the axons from all ipsilaterally projecting cells was  $\sim 270 \mu\text{m}$  (Sup. Table) with the longest reconstructed axon being 683  $\mu\text{m}$ . For all cells in this group, the axon initiation site was far away from the somata, and on average, the initiation site was  $36.6 \pm 12.74 \mu\text{m}$  from the somata.

Dendrites emerged laterally from somata and always extended ventrally. Cells in this group had large dendritic arbors, with the dendrites in this group arborizing over 13.3% of the total imaged volume (Sup. Fig. 4A,B,C). We also found the average dendrite for cells in this group to have significantly larger diameter as compared to the diameter of the axons (Fig. 3B,  $p < 2 \times 10^{-3}$ , ttest, Sup. Table). Only in one case the dendrites were observed to cross the midline, as indicated by the presence of postsynaptic sites (Fig. 3A, Ipsi. only, arrowhead).

Both ipsi- and contralateral projections ("ipsi-contra") - Two cells had axons with both ipsilateral and contralateral projections (Fig. 2C, 3A, ipsi-contra). Integrator cells from this group were located more lateral to the cells from *ipsi-only group*. The ipsilateral projections resembled the axons of ipsi-only group cells (Fig. 3A), with similar tilt in the rostro-caudal axis. In both cells, another neurite crossed the midline. We infer that this neurite is a putative contralaterally projecting axon. This cannot be confirmed with certainty, because its presynaptic sites are on the contralateral side of the hindbrain, outside the imaged volume. Our inference is based on a number of cues as mentioned previously. In both cases, the midline cross-over happened at locations that were ventral to the cells somata. On average the axons (ipsi+putative contra) were  $\sim 270 \mu\text{m}$  long and the dendrites were  $\sim 400 \mu\text{m}$  long. Cells in this group arborized over 4.3% of the total volume (Sup. Fig. 4A,B,C).

*Contralateral projection only (“contra-only”)* - Eight cells located at the caudal most extent of the imaged volume, contained exclusively contralaterally projecting putative axons (Fig. 3A, contra only). Like the axons in the ipsi-only group, the putative contralateral axons did not emerge as axons, but started as a neurite with postsynaptic sites, that became axonal. However, unlike the ipsi-only group, the axon initiation site was much closer to the somata. On average, the axon initiation site was  $12.89 \pm 6.07 \mu\text{m}$  from the somata, which is significantly shorter than the axon initiation site for the ipsi-only group ( $p < 0.0003$ , ttest).

The average dendritic length was  $\sim 290 \mu\text{m}$ , and the arbor volume of these dendrites was significantly smaller than the dendritic arbors of ipsi-only group, ipsi-contra group combined ( $p < 0.003$ , ttest). The average diameter of dendrites significantly larger than the diameter of the axons (Fig. 3B,  $p < 2 \times 10^{-6}$ , ttest), and that diameter of the contra-only cells was significantly smaller to the ipsi-only group (Fig. 3B,  $p < 0.005$ , ttest). Cells in this group arborized over 7.2% of the total volume (Sup. Fig. 4A,B,C).

*Projection unknown (“unknown”)* - The last seven cells were located at the lateral most extent of the volume. For these cells we did not find any neurites with presynaptic sites nor could we locate a putative axon (Fig. 3A, unknown). We believe this is most likely because these cells were not fully represented in the imaged volume and neurites of these cells exit the volume before the axon was located. The average length of the dendrites for cells from this group was  $\sim 220 \mu\text{m}$ , and they occupied on average  $\sim 4.9\%$  of the total volume (Sup. Fig. 4A,B,C).

## 2.5 Numbers and distribution of synapses

On average, cells from these four groups had approximately  $\sim 170$ ,  $125$ ,  $85$  and  $40$  postsynaptic (inputs) sites respectively (Fig. 3C, top, red), and, the axons from the ‘ipsi’ and ‘ipsi-contra’ groups had approximately  $\sim 56$  and  $\sim 30$  presynaptic (output) sites (Fig. 3C, top, green). The number of postsynaptic sites on the ‘ipsi’ group of cells was significantly more than the number of synapses on the ‘contra’ group of cells ( $p = 0.008$ , Wilcoxon-rank test). We then computed the pathlengths of each synaptic location form the somata to determine if there were differences in the distributions of the synaptic locations for each of the groups. The ipsilateral axon form the ‘ipsi’ and ‘ipsi-contra’ group revealed presynaptic sites to have distributions that were statistically weak ( $p = 0.01$ , kstest). However the distributions of the postsynaptic sites on each of the four groups was statistically very strong (Fig. 3C, bottom, distributions, Sup. table, P values).

We further computed the synaptic density, the number of synapses per unit length for all cells, with the assumption that the synapses within each group were uniformly distributed along dendrites. The uniformity assumption was made because the distributions of the locations of postsynapses was found to closely match the location of dendritic arbors (Sup. Fig. 5A). We found that the average the ipsi. group of cells had  $2.6 \pm 1.2$  postsynaptic sites (inputs) every micron, whereas as the ‘contra’ group of cells had  $3.6 \pm 0.7$  postsynaptic sites (inputs) every micron (Fig. 3D, top,  $p = 0.059$ , Wilcoxon-rank test). These differences in synaptic densities is not due to differences in lengths of the dendrites, but reflects actual differences in the underlying location of postsynaptic sites along the dendrites. Empirically the average intersynaptic distance for the ‘ipsi’ and ‘contra’ groups of cells are  $1 \pm 2.3 \mu\text{m}$  and  $1.2 \pm 1.6 \mu\text{m}$  (Fig. 3D, bottom, P values from Wilcoxon-rank test).

## 2.6 Planar organization of dendrites

The dendrites of the cells form the ipsi and contra groups were observed to lie along orthogonal planes. The dendrites of the cells in the ipsi groups were noticed to like roughly along a coronal plane with some tilt (Fig. 3A). Similarly, the dendrites of the cells in the contra cells were noticed to exhibit some planar organization as well. Fitting a plane through the postsynaptic sites that lie along the dendrites of the cells in the ipsi and contra groups revealed that these plane were nearly orthogonal ( $81.34^\circ$ ) to each other (Fig. 4A).

The dendrites arbors of the cells in these two groups displayed an inversion in the stratification depths. The dendritic arbors of the ipsi cells peaked a at a depth of  $38.9 \pm 8.3 \mu\text{m}$  ventral to its cells somata (Fig. 4B, top). Whereas for the contra group the peak stratification depth was around  $12.4 \pm 8.8 \mu\text{m}$  ventral its somata (Fig. 4B, bottom). Interestingly, when the peak locations of all cell somata in the imaged volume is overlaid with the stratification profiles of the dendrites, we see that the dendrites and axons of the ipsi group projected arbors that overlapped with cells along the medial and lateral most peaksWhereas the dendrites of the contra group were located very close the intermediate peak of somata.

## 2.7 Connectivity between integrator neurons

We also examined the patterns of connectivity between integrator neurons. We found that there exists overlap of the axons of the ipsilaterally projecting cells (Sup. Fig. 5B, green) with the dendrites of all other cells in the volume (Sup. Fig. 5B, red). More specifically, the overlap at ventro-rostral locations seems to be from axons of ipsi cells onto dendrites of other ipsi-cells, whereas the overlap at dorso-caudal locations seem to be from axons of ipsi-cells onto dendrites of contra-cells.

Even though there was notable overlap in the axonal and dendritic fields, when looked at in finer resolution we found that there were very few locations where axo-dendritic contacts were made. From the axon collaterals of one integrator cell, we found the hypothesized synapses onto other integrator cells. This single cell belonged to the *ipsi-only* group. It made 2 synapses onto another *ipsi-only* cell and 1 synapse each onto two *contra-only* cells (Fig. 4C). A total of eight cells (*ipsi-only* and *ipsi-contra*) had ipsilaterally projecting axons. Based on this projection pattern, it might appear that all eight cells had the *potential* to make synapses onto other integrator neurons within the confines of the imaged volume. However, this would be overstating the case if the axons failed to even approach dendrites. Therefore we decided to define a “potential synapse” as a location where axon and dendrite approached each other closer than 1  $\mu\text{m}$  [Stepanyants and Chklovskii, 2005]. We found 48 potential synapses between integrator cells (Fig. 4C, inset). Of this set, 40 involved the one cell that made the four real synapses (Fig. 4C, inset, arrow). Therefore this cell seemed exceptional in that it made a disproportionate number of potential synapses as well as all the real synapses. This number dropped substantially if the cell was randomly translated by as little as 5  $\mu\text{m}$  from the postsynaptic cell (Sup. Fig. 5C).

## 3 Discussion

Here we detailed an approach where we recorded from cells in the larval zebrafish that were encoding for a behavioral variable, in this case eye-position, followed by registering the light microscopic images to an electron microscopic volume to locate the same cells. We were able to reconstruct 22 integrator cells for which we had both function and structure. This procedure revealed the existence of distinct groups of cells that make up the ipsilateral integrator circuit. By inferring the neurotransmitter identity of the cells, we show that there are at least two distinct groups of cells in the integrator circuit. An excitatory, ipsilaterally projecting population and an inhibitory contralaterally projecting population. We also find evidence for a third, new, ipsilateral and contralaterally projecting population. Finally we provide the first conclusive evidence for synapses between integrator neurons. This high-throughput approach can be extended to multiple cells in the same animal, to provide rich functional and structural information from multiple cells to understand neural circuits in organisms.

It has long been theorized that positive feedback could be a mechanism that can explain long persistent time scales of neuronal activity. Here we present evidence that the ‘*ipsi*’ group of cells in this study is a strong candidate that can setup positive feedback. Eight of the reconstructed cells had ipsilaterally projecting axons. The somata of almost all the neurons in the *ipsi* group lie within close to the medial most peak of cell somata, making them most likely excitatory. The axons and dendrites of these cells display a planar organization. The majority of its input synapses lie along a plane approximately normal to the rostro-caudal axis. This suggests that these cells are setup to broadly sample from axon that traverse the RC axis. This fact is also evident in the projection pattern of the axons from this group of cells. Its axons travel along the RC axis, and its output synapses lie along a plane approximately normal to its dendrites (Sup. Fig.). Finally, we also observed conclusive chemical synapses from one ipsilaterally projecting integrator cell onto another ipsilaterally projecting integrator cell. These facts point to the *ipsi* group of cells as the most likely candidate for establishing positive feedback in the integrator circuit.

The second major class of cells that we reconstructed were the contralaterally projecting population of cells. In the gold fish oculomotor integrator, contralaterally projecting cells are thought to be involved in coordinating activity between the two sides, and that each side acts as an independent integrator [Aksay et al., 2007, Debowy and Baker, 2011]. Evidence from light microscopic images of contralaterally projecting cells shows axon like projections that terminate close to the opposing population of inhibitory integrator neurons [Lee et al., 2015]. In our study, the contralaterally projecting neurons were located in a loose group at the caudal extent of the imaged volume. The somatic location of these neurons correspond very closely to the intermediate peak of somata, that are largely GABAergic. The dendrites of these neurons arborized over a smaller area, and were stratified more dorsally as compared to the *ipsi* cells. Although, we observed chemical synapses from one ipsilateral neurons onto two contralateral neurons, the

planar organization of all the postsynapses (inputs) onto these cells was orthogonal to the inputs on the ipsilateral neurons. This suggests that these cells sample narrowly from axons along the RC axis.

Our evidence thus suggest that at least two of the groups, the ipsilaterally projecting and the contralaterally projecting neurons are unique populations. They have significantly different morphologies, dendritic arbors and axonal projections patterns. The distributions of postsynapses along the dendrites are significantly different. The ipsi-only group of cells had twice as many postsynaptic sites as the contra-only group. Similarly, the emergence of the axon in the ipsi-only group, is much farther as compared to the contra-only group. This feature could be important to influence the cells, since these locations are most proximal to the somata.

Our sample of 22 reconstructed cells is a fraction of the roughly 100 integrator neurons estimated to exist on one side of the larval zebrafish brain [Aksay et al., 2003]. If the observed synapses are representative of the entire population, this suggests the integrator population contains a subset of cells well-connected with each other. While the remaining cells may serve to communicate eye-position related information to other brain areas [Dai et al., 2015]. On the other hand, this observation may be an underestimate of integrator connectivity, for a few reasons. First, there are many cells in the imaged volume that carried no usable calcium signal at all, largely because they did not take up enough calcium indicator. Some of these cells are likely to be integrator neurons overlooked by our study, and are potential postsynaptic partners of the reconstructed cells in our sample. Second, there are integrator neurons outside the imaged volume, and they could receive synapses from our reconstructed integrator neurons. (Only three axonal arbors were fully or mostly reconstructed; the rest appeared substantially cut off as their axons left the volume.) Third, we had no possibility of finding connections between neurons on opposite sides of the brain, because only one side of the brain was imaged. Therefore, it is difficult to know whether the single cell that made synapses onto other integrator neurons is an exceptional case, or a representative of a larger population that was incompletely sampled.

What remains unknown are the presynaptic partners of these cells, and how do they influence the function of the integrator cell, whether and if there are preferred locations on the dendrite from specific cells. More definitive information about connectivity patterns between integrator cells awaits a future experiment with an imaged volume that is large enough to encompass all integrator cells, and a fluorescent calcium indicator that labels a higher percentage of integrator cells.

## 4 Experimental procedures

### Two-photon calcium imaging.

Anesthetized *nacre* mutant zebrafish larvae was bulk-loaded with calcium sensitive dye Oregon Green 488 BAPTA-1 AM by inserting a capillary through the dorsal skin surface over the lateral edge of the right side of the hindbrain just caudal to the cerebellum, at ~30° decline relative to the dorsal surface. After several hours in order to recover, the animal was imaged on a custom two-photon microscope. The animal was immobilized in low melting agar and was positioned to view a monitor with light gratings. The hindbrain of the animal was imaged at (790 nm) at predefined plane at (0.98 Hz). Following functional imaging, the animal was then imaged on the same setup for anatomical imaging. Briefly, a stack was acquired over the same imaging window, with optical sections every 1.3 μm, and with a lateral resolution of 0.5 μm. Once this was performed, the animal was anesthetized and the skin over the hindbrain was removed, to facilitate penetration of the fixative, and the animal was immersed in fixative to preserve the ultrastructure. We found that the removal of the skin over the hindbrain was important for good ultrastructure preservation and for even staining of the tissue.

### Serial section electron microscopy.

The animal was immersed in a fixative of 1% paraformaldehyde and 1% glutaraldehyde buffered in 0.1M cacodylate buffer for 24 hrs. Then it was thoroughly washed in 0.1M cacodylate buffer before staining. The tissue was stained using a conventional ROTO procedure (Tapia et al. [2012]). Following staining, the tissue was infiltrated with an LX-112 based EPON resin for 24 hrs and baked for 48 hrs at 60 C. Care was taken to orient the specimen to permit sectioning along the horizontal axis. Serial sections from the above animal were collected approximately from the level of the Mauthner cell at a thickness of 45 nm. The serial sections were collected using the automatic tape-collecting ultramicrotome (ATUM) [Hayworth et al., 2014, Kasthuri et al., 2015]. Each wafer was imaged in a Zeiss Sigma field emitting scanning electron microscope in the backscattered electron mode using a custom software interface to collect the images (Hayworth et al. [2014]). The imaged volume was  $220 \times 112 \times 57 \mu\text{m}^3$ . The images were montaged and aligned using the TrakEM2 plugin in FIJI/ImageJ (Cardona et al. [2012]).

### Registration of light microscope and electron microscope volumes

We performed the functional light microscopy at pre-defined planes close to and below the Mauthner cell, unilaterally. This landmark would later serve to identify cells in the electron microscopy volume, since the Mauthner cell is immediately visible in EM sections. Following the functional imaging, the volume was imaged for anatomical landmarks, like blood vessels and location of cell bodies, this volume was termed the light microscopy (LM) volume. We later extracted the locations of cells whose firing had high degree of correlation to eye-position, and had the firing characteristic of neural integrator cells, similar to [Miri et al., 2011b,a, Daie et al., 2015].

Once functional imaging of the larva was performed, it was immediately prepared for serial section electron microscopy, as described above. Each section was imaged at a lateral resolution of 5nm/pixel in a region of interest that roughly corresponded with area imaged on the light microscopic. The EM volume we imaged contained 15791 image tiles (8K x 8K pixels each) or  $\sim 10^{11}$  pixels (Fig. 1B). These images were registered using the trakEM2 plugin in Fiji (Cardona et al. [2012]). Briefly, individual images were first montaged using affine transforms followed by elastic transforms.Reconstructions

The reconstruction of the cells was performed using the TrakEM2 plugin in Fiji/ImageJ. Two expert tracers reconstructed the cells beginning from the cell bodies in an independent manner. During the tracing process, one of the expert tracers annotated all pre and postsynaptic sites for each cells. The skeletonized tree structure was exported from TrakEM2 as \*.swc files. These trees were then imported into Matlab using custom scripts to import .swc files and maintain them as trees. The traces of the two tracers were compared by a third reviewer. The third reviewer, independently reviewed points of disagreement and decided which points of disagreement were either over-reconstructed or were under-reconstructed. In some cases, the traces were re-visited by the tracers if it was needed. For the comparison of EM traces with LM traces, the LM traces were traced using the Simple Neurite Tracer (Longair et al. [2011]) plugin in Fiji, and exported as a \*.swc file. They were then imported into the same Matlab framework that was used to analyze the EM traces, and used to compute necessary features to compare the LM traces and the EM traces. The total length of all reconstructed neurites in the imaged volume was 9.55 mm. In some cases, the neurite of the cells exited the volume and were thus under reconstructed.

#### Analysis

All analysis was performed on Matlab using custom scripts.

To assess the degree of completeness of the cells that were reconstructed, we compared the EM reconstructions of the cells with the long-range axons to previously reported LM reconstructions of similar neurons (Lee et al. [2015]). We did not observe any significant difference in the total number of axonal collaterals and the length of these collaterals (Sup. Fig. 4D,E,F).

To investigate the reliability of such inferences, we quantified the caliber of our axons and dendrites. For 20 out of 22 cells, the mean axonal diameter was less than the mean dendrite diameter, conforming to the textbook notion that axons are thinner than dendrites (addressed later). However, the axon was thicker than the dendrites for the remaining two cells, so inference of neurite identity based on caliber would have been erroneous for these cells.

## 5 Author contributions

Conceptualization, Methodology, and Writing: A.V, E. A., and H.S.S. Formal Analysis: A.V. and H.S.S. Data Curation: A.V. Visualization: A.V. Investigation: K.D performed two-photon calcium imaging. A.V. acquired serial section EM images with assistance from J.W.L., and assembled the resulting image stack. K.D, A.R. registered the calcium images with the EM images. A.V. and E. A. reconstructed neurons with help from Ashleigh Showler and A.R. Supervision and Funding Acquisition: E.A. and H.S.S.

## 6 Acknowledgments

We are grateful to Juan Carlos Tapia, Richard Schalek and Ken Hayworth for assisting us with tissue preparation, the ATUM serial sectioning procedure, and the WaferMapper software for EM imaging. Stefan Saalfeld, Albert Cardona, and Ignacio Arganda-Carreras answered questions about the TrakEM2 plugin for FIJI/ImageJ. Uygar Sümbül assisted with importing skeletons into MATLAB. We thank Heather Sullivan for tissue processing and optimization. We benefited from helpful discussions with David Tank and Kanaka Rajan. HSS acknowledges funding from the Mathers Foundation, Gatsby Foundation, Human Frontier Science Program, NIH/NINDS award 5R01NS076467, and ARO MURI award W911NF-12-1-0594.

---

## References

- Misha B Ahrens, Jennifer M Li, Michael B Orger, Drew N Robson, Alexander F Schier, Florian Engert, and Ruben Portugues. Brain-wide neuronal dynamics during motor adaptation in zebrafish. *Nature*, 485(7399):471–477, May 2012.
- E Aksay, R Baker, H S Seung, and D W Tank. Anatomy and Discharge Properties of Pre-Motor Neurons in the Goldfish Medulla That Have Eye-Position Signals During Fixations. *Journal of Neurophysiology*, 84(2):1035–1049, August 2000.
- E Aksay, G Gamkrelidze, H S Seung, R Baker, and D W Tank. In vivo intracellular recording and perturbation of persistent activity in a neural integrator. *Nature neuroscience*, 4(2):184–193, February 2001.
- Emre Aksay, Robert Baker, H Sebastian Seung, and David W Tank. Correlated discharge among cell pairs within the oculomotor horizontal velocity-to-position integrator. *The Journal of neuroscience : the official journal of the Society for Neuroscience*, 23(34):10852–10858, November 2003.
- Emre Aksay, Itsaso Olasagasti, Brett D Mensh, Robert Baker, Mark S Goldman, and David W Tank. Functional dissection of circuitry in a neural integrator. *Nature neuroscience*, 10(4):494–504, April 2007.
- Michael J F Barresi, Lara D Hutson, Chi-Bin Chien, and Rolf O Karlstrom. Hedgehog regulated Slit expression determines commissure and glial cell position in the zebrafish forebrain. *Development (Cambridge, England)*, 132(16):3643–3656, August 2005.
- Davi D Bock, Wei-Chung Allen Lee, Aaron M Kerlin, Mark L Andermann, Greg Hood, Arthur W Wetzel, Sergey Yurgenson, Edward R Soucy, Hyon Suk Kim, and R Clay Reid. Network anatomy and in vivo physiology of visual cortical neurons. *Nature*, 471(7337):177–182, March 2011.
- Kevin L Briggman, Moritz Helmstaedter, and Winfried Denk. Wiring specificity in the direction-selectivity circuit of the retina. *Nature*, 471(7337):183–188, March 2011.
- Albert Cardona, Stephan Saalfeld, Johannes Schindelin, Ignacio Arganda-Carreras, Stephan Preibisch, Mark Longair, Pavel Tomancak, Volker Hartenstein, and Rodney J Douglas. TrakEM2 software for neural circuit reconstruction. *PLoS ONE*, 7(6):e38011, 2012.
- Alicia Colombo, Germán Reig, Marina Mione, and Miguel L Concha. Zebrafish BarH-like genes define discrete neural domains in the early embryo. *Gene Expression Patterns*, 6(4):347–352, April 2006.
- Kayvon Daie, Mark S Goldman, and Emre R F Aksay. Spatial patterns of persistent neural activity vary with the behavioral context of short-term memory. *Neuron*, 85(4):847–860, February 2015.
- Alexis Dale and Kathleen E Cullen. Local Population Synchrony and the Encoding of Eye Position in the Primate Neural Integrator. *The journal of neuroscience*, 35(10):4287–4295, March 2015.
- Owen Debowy and Robert Baker. Encoding of eye position in the goldfish horizontal oculomotor neural integrator. *Journal of Neurophysiology*, 105(2):896–909, February 2011.
- D Fisher, I Olasagasti, D W Tank, E R F Aksay, and M S Goldman. A modeling framework for deriving the structural and functional architecture of a short-term memory microcircuit. *Neuron*, 79(5):987–1000, 2013.
- Rainer W Friedrich, Gilad A Jacobson, and Peixin Zhu. Circuit Neuroscience in Zebrafish. *Current Biology*, 20(8):R371–R381, April 2010.
- Kenneth J Hayworth, Josh L Morgan, Richard Schalek, Daniel R Berger, David G C Hildebrand, and Jeff W Lichtman. Imaging ATUM ultrathin section libraries with WaferMapper: a multi-scale approach to EM reconstruction of neural circuits. *Frontiers in Neural Circuits*, 8:68, 2014.

Shin-Ichi Higashijima, Gail Mandel, and Joseph R Fethcho. Distribution of prospective glutamatergic, glycinergic, and GABAergic neurons in embryonic and larval zebrafish. *The Journal of comparative neurology*, 480(1):1–18, November 2004.

Shaista Jabeen and Vatsala Thirumalai. Distribution of the gap junction protein connexin 35 in the central nervous system of developing zebrafish larvae. *Frontiers in Neural Circuits*, 7:91, 2013.

M Joshua and S G Lisberger. A tale of two species: Neural integration in zebrafish and monkeys. *Neuroscience*, 296: 80–91, June 2015.

B Yeshwant Kamath and Edward L Keller. A neurological integrator for the oculomotor control system. *Mathematical Biosciences*, 30(3-4):341–352, January 1976.

Narayanan Kasthuri, Kenneth Jeffrey Hayworth, Daniel Raimund Berger, Richard Lee Schalek, José Angel Conchello, Seymour Knowles-Barley, Dongil Lee, Amelio Vázquez-Reina, Verena Kaynig, Thouis Raymond Jones, Mike Roberts, Josh Lyskowski Morgan, Juan Carlos Tapia, H Sebastian Seung, William Gray Roncal, Joshua Tzvi Vogelstein, Randal Burns, Daniel Lewis Sussman, Carey Eldin Priebe, Hanspeter Pfister, and Jeff William Lichtman. Saturated Reconstruction of a Volume of Neocortex. *Cell*, 162(3):648–661, July 2015.

Yukiko Kimura, Yasushi Okamura, and Shin-Ichi Higashijima. alx, a zebrafish homolog of Chx10, marks ipsilateral descending excitatory interneurons that participate in the regulation of spinal locomotor circuits. *The Journal of neuroscience : the official journal of the Society for Neuroscience*, 26(21):5684–5697, May 2006.

Amina Kinkhabwala, Michael Riley, Minoru Koyama, Joost Monen, Chie Satou, Yukiko Kimura, Shin-Ichi Higashijima, and Joseph Fethcho. A structural and functional ground plan for neurons in the hindbrain of zebrafish. *Proceedings of the National Academy of Sciences of the United States of America*, 108(3):1164–1169, January 2011.

Minoru Koyama, Amina Kinkhabwala, Chie Satou, Shin-Ichi Higashijima, and Joseph Fethcho. Mapping a sensory-motor network onto a structural and functional ground plan in the hindbrain. *Proceedings of the National Academy of Sciences of the United States of America*, 108(3):1170–1175, January 2011.

Melanie M Lee, Aristides B Arrenberg, and Emre R F Aksay. A Structural and Genotypic Scaffold Underlying Temporal Integration. *The journal of neuroscience*, 35(20):7903–7920, May 2015.

R K Lee, R C Eaton, and S j Zottoli. Segmental arrangement of reticulospinal neurons in the goldfish hindbrain. *The Journal of comparative neurology*, 329(4):539–556, March 1993.

WCA Lee, V Bonin, M Reed, B J Graham, and G Hood. Anatomy and function of an excitatory network in the visual cortex. *Nature*, 2016.

R John Leigh and David S Zee. *The Neurology of Eye Movements*. Oxford University Press, USA, June 2015.

Mark H Longair, Dean A Baker, and J Douglas Armstrong. Simple Neurite Tracer: open source software for reconstruction, visualization and analysis of neuronal processes. *Bioinformatics*, 27(17):2453–2454, September 2011.

Guy Major and David Tank. Persistent neural activity: prevalence and mechanisms. *Current opinion in neurobiology*, 14(6):675–684, December 2004.

R A McCrea and R Baker. Cytology and intrinsic organization of the perihypoglossal nuclei in the cat. *The Journal of comparative neurology*, 237(3):360–376, July 1985.

Andrew Miri, Kayvon Daie, Aristides B Arrenberg, Herwig Baier, Emre Aksay, and David W Tank. Spatial gradients and multidimensional dynamics in a neural integrator circuit. *Nature neuroscience*, 14(9):1150–1159, September 2011a.

Andrew Miri, Kayvon Daie, Rebecca D Burdine, Emre Aksay, and David W Tank. Regression-Based Identification of Behavior-Encoding Neurons During Large-Scale Optical Imaging of Neural Activity at Cellular Resolution. *Journal of Neurophysiology*, 105(2):964–980, February 2011b.

Freda Newcombe. Neuropsychology quainterface. *Journal of Clinical and Experimental Neuropsychology*, 7(6):663–681, January 2008.

A M Pastor, R R De la Cruz, and R Baker. Eye position and eye velocity integrators reside in separate brainstem nuclei. *Proceedings of the National Academy of Sciences*, 91(2):807–811, January 1994.

Ronald S Petralia, Ya-Xian Wang, Mark P Mattson, and Pamela J Yao. Structure, Distribution, and Function of Neuronal/Synaptic Spinules and Related Invaginating Projections. *NeuroMolecular Medicine*, 17(3):211–240, May 2015.

D A Robinson. Integrating with neurons. *Annual review of neuroscience*, 1989.

J Rosenbluth and S L Palay. The fine structure of nerve cell bodies and their myelin sheaths in the eighth nerve ganglion of the goldfish. *The Journal of biophysical and...*, 1961.

H S Seung. How the brain keeps the eyes still. *Proc. Natl. Acad. Sci. USA*, 93(23):13339–13344, 1996.

H Sebastian Seung, Daniel D Lee, Ben Y Reis, and David W Tank. Stability of the Memory of Eye Position in a Recurrent Network of Conductance-Based Model Neurons. *Neuron*, 26(1):259–271, April 2000.

H J Steiger and J A Büttner-Ennever. Oculomotor nucleus afferents in the monkey demonstrated with horseradish peroxidase. *Brain research*, 160(1):1–15, January 1979.

A Stepanyants and D Chklovskii. Neurogeometry and potential synaptic connectivity. *Trends in neurosciences*, 28(7):387–394, July 2005.

Juan Carlos Tapia, Narayanan Kasthuri, Kenneth J Hayworth, Richard Schalek, Jeff W Lichtman, Stephen J Smith, and JoAnn Buchanan. High-contrast en bloc staining of neuronal tissue for field emission scanning electron microscopy. *Nature Protocols*, 7(2):193–206, February 2012.

A M van Alphen, J S Stahl, and C I De Zeeuw. The dynamic characteristics of the mouse horizontal vestibulo-ocular and optokinetic response. *Brain research*, 890(2):296–305, February 2001.

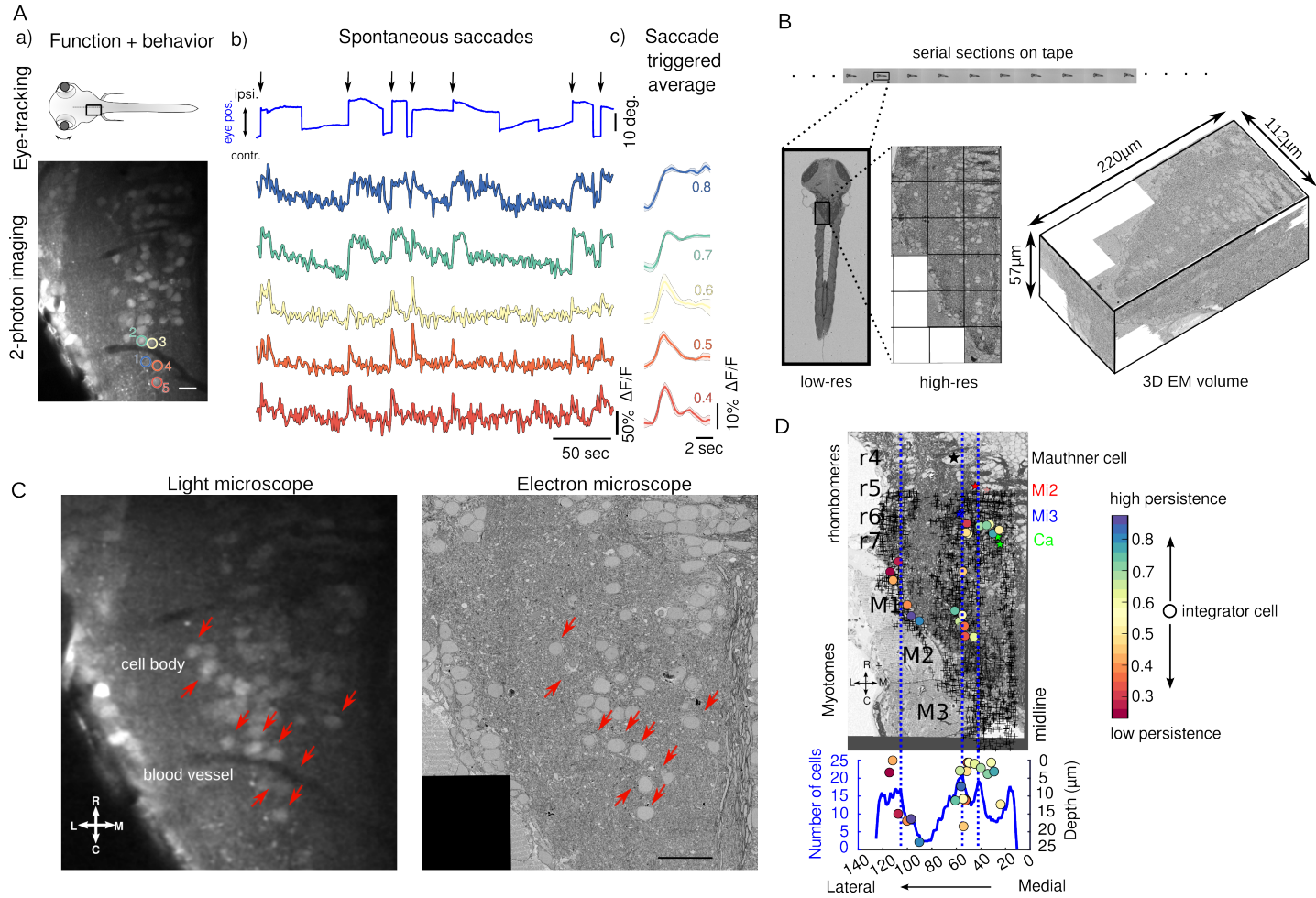


Figure 1: Functional and structural imaging of integrator cells.

(A) (a) Top - Larval zebrafish schematic showing the region where functional imaging was performed (black box) located in the hindbrain, along with recording of eye-tracking behavior.

Bottom - A single imaging plane showing cells loaded with calcium indicator OGB-1. Identified integrator cells are shown in colored circles. Colors reflect the level of persistence of the cell as in (c). Scale bar 20  $\mu$ m

(b) Spontaneous eye movement (top, blue line) showing saccades (sharp vertical lines) and post-saccadic fixations (horizontal lines). Ipsilateral saccades are indicated by black arrows. Colored traces are the changes in fluorescence from individual cells from imaging plane in (a). Color coding represent the normalized persistence level of the cell (c).

(c) Normalized fluorescence response following saccades. Thick line shows the average, with shaded region showing the SEM. Colored numbers, is the average under the curve of the normalized fluorescence responses which indicate the persistence of the cell.

(B) Serial electron microscopy of same zebrafish from A, serial-sections are collected on tape in an automated manner, images at low-resolution are used to align the sections, imaging at high-resolution over the defined region of interest (black box) gives final 3D-EM volume of the imaged area.

(C) Registration of LM volume to EM volume to locate the cells that were involved in the behavior. Red arrows indicate the same features in both LM and EM. Scale bar 20  $\mu$ m

(D) Single EM plane showing anatomical landmarks, Mauthner cell, Mi2, Mi3 and Ca (colored stars). Anatomical location of all integrator cells (colored circles) identified in the behavior and all remaining somata in the imaged EM volume ('+' symbol). Colors of the cells correspond to the persistence level of the cell. Lower panel is a distribution of all cells with integrator cells overlaid. Dotted line corresponds with hindbrain stripes with known neurotransmitter identities.

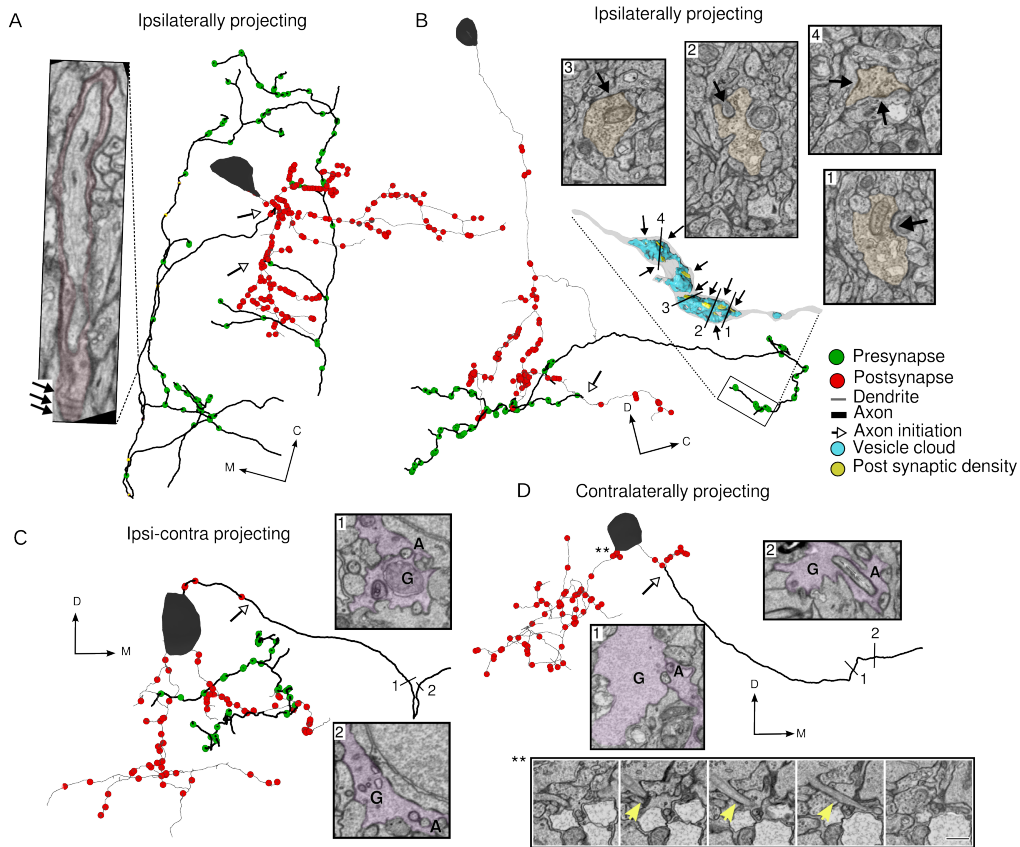


**Figure 2: Integrator cell anatomical features reconstructed from EM volume.**

(A) Example integrator cell showing ipsilaterally projecting axon (dark segment) and dendrite (light segment) with pre- (green circles) and postsynaptic (red circles) locations. Parts of the axon of this integrator cell are loosely-myelinated (colored boxes). Insets show one such myelinated region, with arrows showing individual myelin sheaths that are oblique to the imaging plane. Open arrow heads show the location of axon initiation zones along the neurite.

(B) Integrator cell, with ipsilateral projecting axon that starts as single neurite that branches to give rise to axon and dendrites. Axon is studded with presynaptic sites that are clustered along neurite. Inset is a 3D reconstruction of axon termination zone with a large vesicle cloud (blue) with multiple post synaptic densities (yellow) opposed to the vesicles. Numbers correspond to EM insets showing the synapses. M - Mitochondria, V - Vesicles. Arrows show the synapses at those locations.

(C) Example integrator cell with both ipsi and contralateral projecting axon. Putative contra axon is engulfed by glial process just before crossing the midline. Number correspond to EM insets with colored segments that are glia G, and non-colored segment is axon A. Open arrowhead shows the axons initiation site.

(D) Contralaterally projecting integrator cell with putative axon crossing the midline with glial engulfment (EM insets at numbered locations G - Glia, A - Axon). Bottom EM inset panel shows primary cilium highlighted with yellow arrow. Note all the integrator somata in this volume give rise to a cilium, but it is shown for this cell.

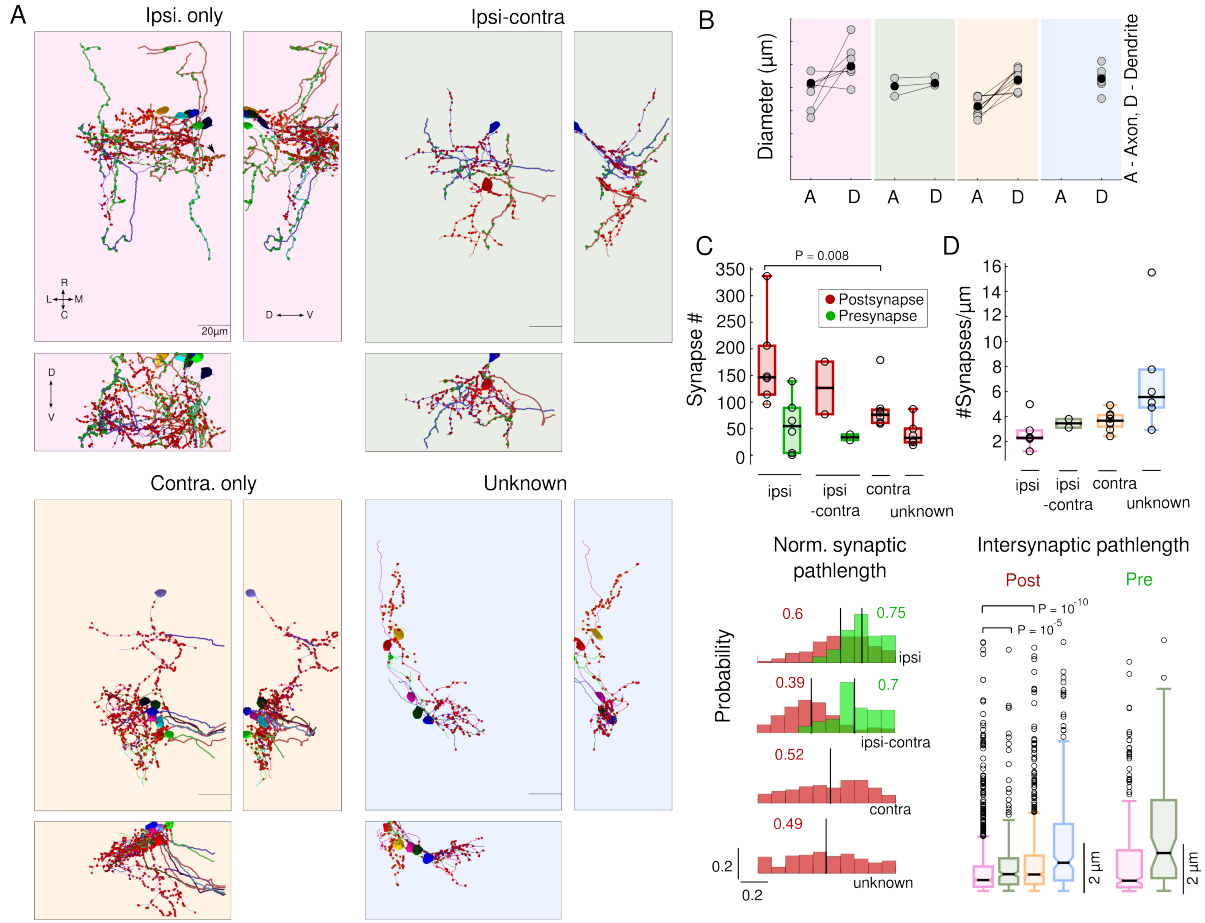


Figure 3: Integrator cells axonal projection patterns and synaptic distribution.

(A) Colored panels show three views of reconstructed cells grouped according to their axonal projection patterns. Top left, 6 integrator cell with ipsilateral projecting axons - ipsi-only group, pink background. Top right, 2 integrator cells with ipsilaterally and putative contralateral projection – ipsi-contra, green background. Bottom left, 8 integrator cells with midline crossing contralateral only putative-axon – contra-only, orange background. Bottom right, 7, integrator cells with unknown axonal projection – unknown, blue background. On the neurites, red circles - postsynaptic sites, green circles - presynaptic sites.

(B) Axonal and dendritic diameter of all cells in each of the four groups. Grey dots are averages for each cell and black dots are averages per group. A - Axon, D - Dendrite.

(C) (Top) Box plot of the number of synapses in each group. Black line is the median (significance reported as Wilcoxon rank-sum test).

(Bottom) Normalized distribution of the synaptic pathlength. Red - postsynaptic sites, green - Presynaptic sites. Black vertical lines, with adjoining colored numbers represent the means of the distribution..

(D) (Top) Box plot of the Synaptic densit, for postsynaptic sites for each group. Black lines are the medians.

(Bottom) Box plots of the intersynaptic path length for all four groups (significance reported as Wilcoxon rank-sum test).

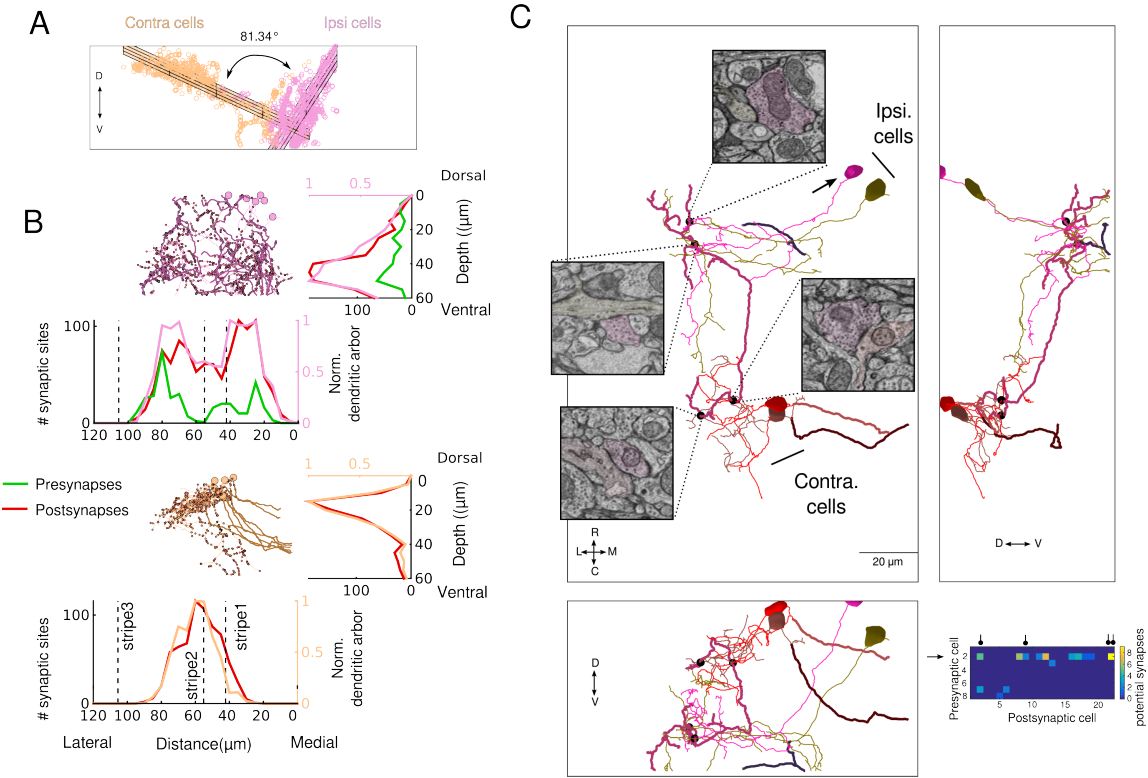


Figure 4: Integrator cells are synaptically connected.

(A) Planar organization of postsynaptic sites on the ipsi (pink) and contra (orange) cells. Grid represent the best fit fit plane through the cloud of points for each group.

(B) (Top) Stratification profile of all ipsi group of cells. Two side vies show the stratificatin of the dendrites, pre and postsynaptic sites along the dorso-ventral and medio-lateral axis. Dotted line represent the location of the somatic peaks that was computed in Figure 1.

(Bottom) Stratification profile of all contra group of cells.

(C) Three views of synaptically connected integrator cells. All synapses were from one cell (magenta, arrow) in ipsi-only group onto one other cell from ipsi-only group (olive). One synapse each from ipsi-only group cell (magenta) onto two contra-only cells (red and brown). Black dots represent the location of the synapses, with insets showing the electron micrograph at the respective location. In all electron micrographs.

(inset) Potential synapses that are  $< 1 \mu\text{m}$  from each other. Cell # 2 (arrow), is the same cell in (A, magenta) that makes maximum number of potential synapses onto other cells and makes the real synapses shown in (A). The real synapses are represented by the black circle in the header.